Theoretical Study of Adsorption of $O(^3P)$ and H_2O on the Rutile $TiO_2(110)$ Surface

Zheng-wang Qu* and Geert-Jan Kroes

Leiden Institute of Chemistry, Gorlaeus Laboratories, Leiden University, Post Office Box 9502, 2300 RA Leiden, The Netherlands

Received: August 4, 2006; In Final Form: September 13, 2006

The adsorption of oxygen atoms [$O(^3P)$] on both ideal and hydrated rutile $TiO_2(110)$ surfaces is investigated by periodic density functional theory (DFT) calculations within the revised Perdew−Burke−Ernzerhof (RPBE) generalized gradient approximation and a four Ti-layer slab, with (2×1) and (3×1) surface unit cells. It is shown that upon adsorption on the TiO_2 surface the spin of the O atom is completely lost, leading to stable surface peroxide species on both in-plane and bridging oxygen sites with O-binding energies of about 1.0−1.5 eV, rather than to the kinetically unstable terminal Ti−O and terminal O−O species with smaller binding energies of 0.1−0.7 eV. Changes in O-atom coverage ratios between $^1/_3$ and 1 molecular layer (ML) and coadsorption of H_2O have only minor effects on the O-binding energies of the stable peroxide configurations. High O-atom diffusion barriers of about 1 eV are found, suggesting a slow recombination rate of adsorbed O atoms on $TiO_2(110)$. Our results suggest that the TiOOTi peroxide intermediate experimentally observed in photoelectrolysis of water should be interpreted as a single spinless O adatom on TiO_2 surface rather than as two Ti−O$^\bullet$ radicals coupled together.

I. Introduction

The photoelectrolysis of water at the surface of semiconductor metal oxides such as TiO_2 may, as a part of photoelectrolysis of water, provide hydrogen as a clean and sustainable energy carrier from solar energy.[1] This process has therefore attracted much attention since its discovery in the early work of Fujishima and Honda.[2] Advantages of TiO_2 semiconductor catalysts are that they are inexpensive and chemically and biologically inert,[3] they are very stable under illumination for water photolysis, and the photoactivity of TiO_2 can be extended from the ultraviolet to the visible part of the solar radiative field by chemical doping[3−7] and/or by using TiO_2 nanotube arrays.[8] Furthermore, photochemistry at the surface of TiO_2 also finds application in the removal of organic pollutants in water.[9] Among the natural TiO_2 crystals of rutile, anatase, and brookite, the rutile form is thermodynamically most stable under ambient conditions,[10] and the stable rutile $TiO_2(110)$ surface has been considered as a prototype system in surface science studies of metal oxides and oxide-supported catalysts.[11,12]

To improve the efficiency and stability of photocatalysts for water oxidation, it is quite important to clarify the detailed mechanism of the photooxidation of water on metal−oxide surfaces, especially the involved chemical steps that could be related to the high oxygen-evolving overpotential. Recent experimental data have suggested that the photoevolution of oxygen should be initiated by the nucleophilic attack of a H_2O molecule on a surface-trapped hole,[13−15] leading to intermediates such as surface [Ti−O$^\bullet$, TiOH] pair, TiOOTi, and TiOOH. In particular, the peroxide TiOOTi intermediate is proposed to be formed from two adjacent Ti−O$^\bullet$ radicals or the further oxidation of the [Ti−O$^\bullet$, TiOH] pair on bridging sites. From the theoretical point of view, it is thus crucial to understand these surface structures and detailed reaction steps. However, our knowledge about such mechanistic details is still far from clear: there is even much recent debate on the adsorption structures of water[16−18] and the mobility of oxygen species[19−24] on TiO_2 surfaces. Note that recent theoretical studies[21−24] on the mobility of O_2 on reduced $TiO_2(110)$ were mainly inspired by the alleged experimental observation of O_2-mediated diffusion of surface O-vacancies,[19] which recently turned out to involve H_2O dissociation and diffusion instead.[25]

In this theoretical study, we concentrate on the adsorption and mobility of oxygen adatoms on the ideal $TiO_2(110)$ surface and possible coadsorption structures with water, which is crucial for understanding the detailed mechanism of water electrolysis and photoelectrolysis on metal oxide surfaces. The latter topic (coadsorption of O and H_2O) is also somewhat related to recent studies on the O-adatom-induced water dissociation on the TiO_2-(110) surface.[26,27]

II. Computational Procedures

All the density functional theory (DFT) calculations are performed within the generalized gradient approximation (GGA) by use of the revised Perdew−Burke−Ernzerhof (RPBE) functional[28] and by use of Vanderbilt ultrasoft pseudopotentials[29] for the ionic cores and plane-wave basis sets[30,31] describing the H 1s, O 2s and 2p, and Ti 3s, 3p, 3d, 4s and 4p valence shells, as implemented in the DACAPO program in the ASE[32] package. Note that the Ti 4p shell is included for a better description of the chemical bonding, although it is not occupied in the ground state of Ti atom. Plane-wave basis-set cutoffs for the smooth part of the wave functions and the augmented density are 340 and 500 eV, respectively. A Fermi smearing of 0.1 eV and Pulay mixing is used to ensure fast convergence of the self-consistent electron density.

The rutile TiO_2 bulk lattice constants are optimized by use of $8 \times 8 \times 8$ Monkhorst−Pack-type *k*-point sampling for the crystal unit cell. The optimized lattice constants *a* and *c* of the

* Corresponding author: e-mail z.qu@chem.leidenuniv.nl.

10.1021/jp065028x CCC: $33.50 © 2006 American Chemical Society
Published on Web 10/26/2006

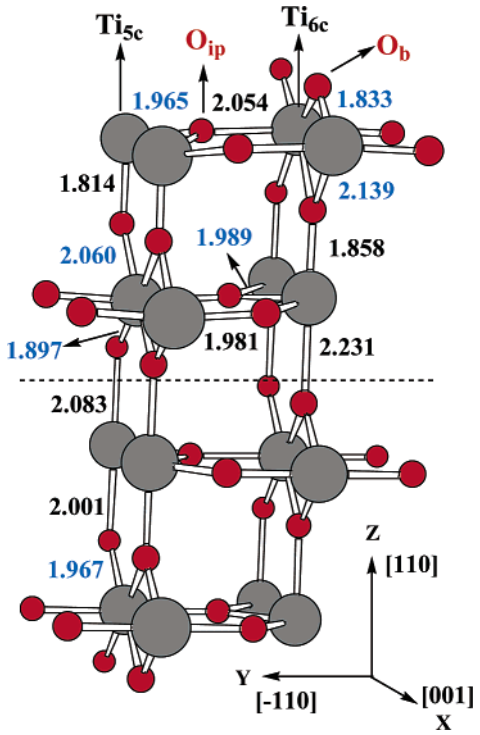

Figure 1. Four Ti-layer slab model used with the (2 × 1) rutile TiO_2 (110) surface unit cell (5.976 Å × 6.562 Å). Gray balls represent titanium atoms, and small red balls represent oxygen atoms. Ti−O bond lengths (in angstroms) along the [110] and [−110] directions are labeled by black numbers, and the others by blue numbers. The two bottom trilayers (below the dashed line) are fixed at the RPBE optimized bulk lattice geometries ($a = b = 4.640$ Å, $c = 2.988$ Å, and $u = 0.305$). The optimized geometries in the (3 × 1) surface unit cell are very similar (within 0.002 Å) and thus are not shown here.

tetragonal TiO_2 bulk unit cell are 4.640 and 2.988 Å, respectively, and the dimensionless parameter u (determining the distances between Ti and O atoms) is 0.305. All these numbers are within 1% of the experimental[33] values of 4.594 and 2.958 Å and 0.305, respectively. According to a rule of thumb, the k-point number times the cell length (in angstroms) in each direction should be larger than about 10 for semiconductors such as rutile TiO_2. We have therefore used a very large k-point mesh to determine the bulk lattice constants.

Periodic four Ti-layer slabs separated by vacuum layers of about 20 Å are chosen to simulate the most stable rutile TiO_2-(110) surface as shown in Figure 1. There are four kinds of surface atoms, that is, 5- and 6-fold-coordinated titanium atoms (Ti_{5c} and Ti_{6c}, respectively), 2-fold-coordinated bridging oxygen (O_b), and 3-fold-coordinated in-plane oxygen (O_{ip}), with the Ti_{5c} and O_b atoms forming surface troughs and ridges along the [001] direction, respectively. We use both 2 × 1 and 3 × 1 surface unit cells (i.e., two and three O_b atoms along the [001] direction, respectively, and one Ti_{5c} atom along the [−110] direction) and 2 × 2 × 1 (along the [001], [−110], and [110] directions) Monkhorst−Pack k-point sampling in the slab calculations. Due to the large size of the 2 × 1 and 3 × 1 surface cells (5.976 × 6.562 × 32.81 Å and 8.964 × 6.6562 × 32.81 Å, respectively), the 2 × 2 × 1 k-point mesh is large enough, as confirmed by the fact that the calculated slab geometries for 2 × 1 and 3 × 1 surface cells are very close (within 0.002 Å). An even smaller Γ-point mesh was shown[22,24] to be enough elsewhere for the TiO_2(110) 2 × 1 surface unit cell.

The two bottom layers are fixed by optimized bulk lattice constants while the two top layers (along with possible adsorbed O atoms and H_2O molecules) are fully relaxed by the quasi-Newton method until the sum of the absolute forces is less than 0.05 eV/Å. This partial relaxation method has been shown to reach better convergence of surface properties with reduced effort, by avoiding the odd−even oscillation problem in full slab relaxation.[34] To get some insights into transition state structures and interconversion barriers, we use the quasi-Newton method with small initial maximum displacement radius of 0.02 Å to get a good initial Hessian and Bofill Hessian updates[35] to find saddle points. For mapping the reaction paths we have based our approach on some previous results[21−23] from the so-called nudged elastic band method. The partial breaking and forming of bonds within the transition-state structures provide further hints for determining the minima they connect to.

The role of spin-polarization is carefully tested in our calculations. It turns out to be important only for free radicals and loosely bound O_2 on TiO_2 with very long Ti···O distances, as will be discussed later. For the species O_2 and O, the energies without spin-polarization are found to be 1.10 and 1.97 eV higher than those with spin-polarization, respectively. For the O_2 ($^3\Sigma_g$) molecule, with the same parameters (see above), the calculated bond length of 1.239 Å and bond energy (without zero-point energy) of 5.33 eV agree well with the experimental[36] values of 1.208 Å and 5.36 eV, respectively. The good agreement for the bond energy is somewhat fortuitous: with triple-ζ atomic basis functions, the RPBE functional somewhat overestimates the O−O bond energy by 0.2 eV.[37] However, Perdew−Wang-91 (PW91), Perdew−Burke−Ernzerhof (PBE), and local-density approximation (LDA) functionals tend to overestimate the O−O bond energy by more than 0.9 eV.[28,37] When O atoms tightly bond to surface Ti and O atoms, their spin magnetic momenta are found to be completely lost, and thus cheaper spin-unpolarized calculations are always appropriate to get the same results.

Since we are mostly interested in the stability of the O adatom as a possible photolysis intermediate on the TiO_2 surface, we have chosen the triplet rather than the more energetic singlet O atom, and free slab (with possible coadsorbed water) as reference systems (energy zero). As will be shown later, though the recombination of O atoms to form O_2 is thermodynamically feasible, it is hindered by high diffusion barriers of about 1 eV. The O-atom adsorption energies E_{ad} are defined as

$$E_{ad} = E(\mathrm{O}) + E(\mathrm{slab}) - E(\mathrm{O} + \mathrm{slab})$$

where E(O), E(slab), and E(O + slab) are the total energies of the free O atom, free slab, and the slab with O adatom, respectively. Note that energies without zero-point corrections are used in the following discussion.

III. Results and Discussion

A. Relaxed TiO_2 (110) Surface. In addition to the good O_2 bond energy and TiO_2 bulk structures obtained in our calculations, an examination of the relaxed free TiO_2(110) surface structures also provides a further test of the quality of our DFT calculations. As shown in Figure 1, the calculated geometries are essentially the same (within 0.002 Å) for the 2 × 1 and 3 × 1 surface unit cells. In TiO_2 bulk, different Ti−O bond lengths of 2.001 and 1.967 Å are found within and between TiO_2Ti four-member rings, respectively. According to our calculations, the in-plane Ti−O bonds of both top layers show similar patterns and values close within 0.06 Å to the bulk values. However, the Ti−O bonds of both top layers within the vertical [−110] planes are evidently different from those of bulk TiO_2. For example, from surface toward bulk, the Ti−O bonds are

alternately shortened and elongated by 0.1∼0.2 Å within the top two layers, with the surface bridging $Ti_{6c}-O_b$ and vertical $Ti_{5c}-O$ bonds shortened by 0.13 and 0.19 Å, respectively. Although further experiments are still needed to verify the alternate shortening and elongation of these bonds, our calculated displacements normal to the surface of Ti_{5c}, Ti_{6c}, O_b, and O_{ip} (−0.08, 0.34, 0.12, and 0.30 Å) with respect to their bulk positions agree reasonably with the recent low-temperature low-energy electron diffraction (LEED)[38] measurements (-0.19 ± 0.03, 0.25 ± 0.03, 0.10 ± 0.05, and 0.27 ± 0.08 Å, respectively).

Partially reduced TiO_2 (110) surfaces were modeled by removing one of the O_b atoms from the 2×1 and 3×1 surface unit cells. Compared with the ideal (110) surface, the most evident structural changes are the inward relaxation by 0.26 Å of the two Ti atoms at the O_b vacancy site and the outward relaxation by 0.32 Å of the oxygen atom below. In addition, the Ti···Ti distance at the O_b vacancy is 0.29 Å longer than that in the ideal surface. The calculated O_b vacancy formation energies per O atom [under the assumption that $O_2(^3\Sigma_g)$ is formed] with the 2×1 and 3×1 surface unit cells are 3.96 and 3.23 eV, respectively, suggesting repulsive interactions between O_b vacancies. Compared with recent DFT calculations with the same 2×1 and 3×1 slab models, our RPBE-calculated vacancy formation energies are about 0.3, 0.3, and 0.8 eV lower than recent PW91,[21] PBE,[24] and LDA[35] results, respectively, possibly due to the fact that the latter functionals overestimate the bond energy of O_2.[28,37]

B. Oxygen Atoms Adsorbed on the TiO_2(110) Surface. We have studied a number of adsorption configurations of O atoms on the TiO_2(110) surface, with the optimized geometries shown in Figure 2. The main structural features with both a single O atom adsorbed on the 3×1 surface unit cell and two O atoms adsorbed on the 2×1 surface unit cell [corresponding to O-atom coverage ratios of $^1/_3$ molecular layer (ML) and 1 ML, respectively, if it is assumed that only Ti_{5c} atoms act as adsorption sites] in "pure" adsorption configurations **a**−**f** are quite similar to those obtained with a single O atom adsorbed on the 2×1 surface unit cell ($^1/_2$ ML). Therefore, our discussions are based on the $^1/_2$ ML results unless mentioned explicitly, while pointing out the effects of lower and higher O-atom coverage ratios for the former case. Note that the configurations **a**−**d** and **f**−**h** have also been found in the literature without specification of structural details,[21−24] while the configurations **e** and **e′** are newly found in our calculations. Also note that in our calculations the relaxed slab with a free $O(^3P)$ atom is taken as the zero of energy.

The configuration **a** is obtained when one O atom is adsorbed exactly on top of a surface Ti_{5c} atom, with a small binding energy of only 0.46 eV. Upon O-atom adsorption, the Ti_{5c} atom is relaxed outward by 0.73 Å while the O atom below it inward by 0.17 Å, leading to a broken Ti···O bond (2.719 Å) and a short surface terminal Ti═O double-bond (1.675 Å) above. As can be seen from Figure 2, the Ti···O distance in **a** decreases with increasing O-atom coverage ratios, while the terminal Ti═O length increases. The O-atom adsorption energy is also quite sensitive to the coverage ratio: it increases to 0.73 eV for the lowest coverage of $^1/_3$ ML, but decreases to only 0.02 eV for the highest coverage 1 ML. However, these values are still much smaller than the recently reported[23] value of 1.9 eV with unknown technical details such as functional and slab relaxation. It is interesting to note that although only slightly elongated the terminal Ti═O bond within **(a)** is much weaker than those found in pure $(TiO_2)_n$ ($n = 1-9$) clusters (∼1.63 Å) with bond energies of about 6 eV.[39]

In both configurations **b** and **c**, one or two Ti_{5c} atoms are also involved as O-atom binding site, but now with additional peroxide single O−O bonding (1.44−1.48 Å) with surface O_{ip} and O_b atoms, respectively, and with longer Ti−O single-bonds (1.91−2.16 Å). Note that in case **c** the Ti_{5c} atom is relaxed outward and the O_b atom involved in bonding tilts out of the plane spanned by the [110] and [001] directions (Figure 1), the added structural constrains leading to slightly less favorable bonding (1.14 eV) than that in case **b** (1.35 eV). Another peroxide configuration **(d)** has structural features and an O-atom adsorption energy (1.30 eV) very similar to those of **b**, but now its O adatom is bound to two Ti_{6c} atoms and one O_b atom with the new O−O bond being parallel to the surface in the [−110] direction. In contrast to the case of the Ti_{5c}-on-top configuration **(a)**, the O-atom adsorption energies of all peroxide configurations **b**−**d** are quite independent (with changes within 0.25 eV) on the O-atom coverage from $^1/_3$ to 1 ML. Our RPBE calculated energy differences between configurations **a**−**d** are consistent with the recent best PW91 calculations[21] with a large c(6×2) surface unit cell (0.17 ML).

Two new peroxide configurations, **e** and **e′**, are found in our calculations, both with the O adatom bound to one bridging $Ti_{6c}-O_b$ bond to form a new TiOO three-membered ring. The O adatom is roughly above the Ti_{6c} atom in configuration **e** but evidently in a tilted configuration in **e′**, with very close O-atom adsorption energies of 0.98 and 1.17 eV, respectively. Interestingly, both **e** and **e′** are found to be rather flexible with a small barrier of 0.2 eV between them, which may provide an easy way for the O adatom to cross the surface O_b ridge to which it binds (but see below). The O-atom adsorption energies of **e** and **e′** are comparable to those found for the other peroxide species **b**−**d** and are also insensitive to further decrease of O-atom coverage ratios from $^1/_2$ to $^1/_3$ ML.

For configuration **f**, with one O atom adsorbed exactly on top of one O_b atom, we find a very small binding energy of only 0.18 eV, although the new O−O bond length (1.36 Å) is about 0.1 Å shorter than those found in peroxide configurations **b**−**e′**. Such weak O−O bonding may not exist when the zero-point energy (about 0.2 eV in free O_2) is taken into account. Structures **d**, **e**, and **e′**, with O_2 adsorbed on an O vacancy site, are more stable than **g** and **h**; this suggests that the lower stability of **f** as compared with **g** and **h** could be due to its terminal O−O bonding and possibly delocalization of electrons associated with the O vacancy over neighboring Ti sites.

Next, we consider two cases (**g** and **h**) where the O atom adsorbed to the ideal surface may be viewed as an O_2 molecule adsorbed to the surface with an O vacancy on it. Compared with the free TiO_2 surface, the O_b vacancy and surface O_2 species cause extensive surface structural deformation, leading to very small effective O-atom binding energies of only 0.30 and 0.46 eV for configurations **g** and **h**, respectively. Thus, although an O_2 molecule may bind to or near an O vacancy, as in configurations **f**−**h** with O_2 binding energies of about 1.5−1.6 eV (defined with respect to relaxed slab with a vacancy and a free O_2 molecule), one O atom could be easily removed from these unstable structures. Our test calculations show that the energies of configurations with an O vacancy are very sensitive to the surface unit cell size. For example, the O_2 binding energy near the O vacancy in configuration **g** is increased by 0.75 eV upon changing from the 2×1 to the 3×1 surface unit cell. This suggests that a large surface unit cell would be required to model the chemistry of TiO_2 surface O

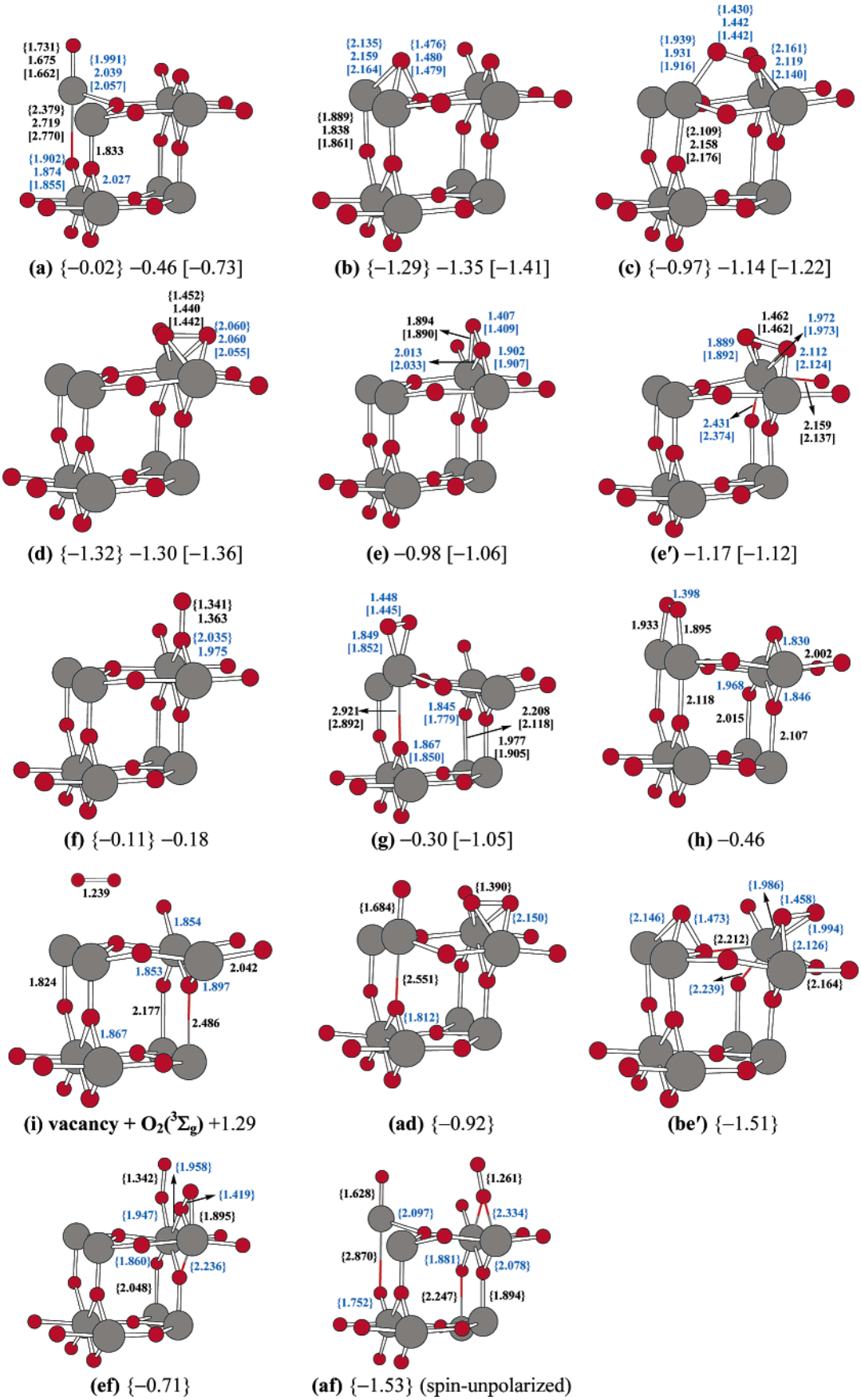

Figure 2. Optimized geometries (in angstroms) and relative energies (in electronvolts) on the rutile (110) surface. Results from two O(^{3}P) atoms on the 2 × 1 surface unit cell are enclosed in braces, and those from single O(^{3}P) atom on the 2 × 1 and 3 × 1 surface unit cells are given without enclosures and with brackets, respectively. The two fixed bottom trilayers of the four-layer model slab are omitted for simplicity. The free slab with free O(^{3}P) atom is taken as zero energy. The combinational adsorption mode of types **a** and **d** on 2 × 1 surface unit cell is labeled as **ad**, and so on.

vacancies. However, O_b vacancies are chemically too reactive to exist in any aqueous solution[40,43] and thus will not be considered further in our study.

Using the 2×1 surface unit cell and 1 ML coverage, we further examine the effect of "mixed" adsorption of O atoms on the $TiO_2(110)$ surface. Some examples are given as configurations **ad**, **be′**, **ef**, and **af** in Figure 2. In configuration **ad**, the structural features are just the combination of "pure" configurations of **a** and **d**, and even the O-atom binding energy (0.92 eV) is approximately the average of those of **a** and **d**. The O-atom binding energy (0.71 eV) of configuration **ef** is also found between those of **e** and **f**. It should be pointed out that several attempts to get 1 ML coverage of configuration **e** on the 2×1 surface unit cell always led to the "mixed" configuration **ef**. The O-atom binding energy (1.51 eV) of the "mixed" configuration **be′** is somewhat lower than those of both **b** and **e′**. It should be pointed out that spin-polarization may become very important at such high O-atom coverage. For example, in pure configurations **a** and **f** at both $^1/_2$ and $^1/_3$ ML coverage ratios, we get the same result with and without spin-polarization. However, although the "mixed" configuration **af** could be found without spin-polarization with a large O-atom binding energy of 1.53 eV as shown in Figure 2, further optimization with spin-polarization (as implemented in the DACAPO program in the ASE package[32]) always led to O_2 elimination at Ti_{6c} sites. This is due to the fact that open-shell structures are more stable for the O_2 entity [as present in the O_2 ($^3\Sigma_g$) product; note that structure **af** contains the O_2 entity]. Thus, caution is always needed for the theoretical modeling of adsorption to complicated oxide surfaces such as TiO_2.

From the discussion above, it is clear that the O atom may be easily adsorbed between surface Ti and O atoms forming stable peroxide species, rather than forming terminal Ti−O and O−O bonds and O_2 species near O vacancies. At first glance, this may be surprising because usually molecules such as H_2O and NH_3 prefer the Ti_{5c} sites for adsorption. However, all these molecules are closed-shell molecules with electron lone pairs, while O atoms are electron-deficient species. It is thus not surprising at all that O atoms approach negatively charged surface O atoms of TiO_2 to first gain negative charge and then also attract positively charged Ti ions in peroxide-type bonding. Interestingly, although the terminal-O configuration **a** is shown to be about 0.6−1 eV less stable than the peroxide configurations on semiconducting $TiO_2(110)$ surface, it is the most stable one on several metal (111) surfaces[41] and on the metallic oxide $RuO_2(110)$ surface,[42] which also has rutile structure. Note that other authors have also discussed configuration **b**−**f** in terms of O_2 bonding to $TiO_2(110)$ with a vacancy on it, whereas we find it more appropriate to discuss the O atom as being part of a peroxide structure.

It should also be pointed that even the most stable peroxide configurations such as **b** and **d** are thermodynamically at least 1 eV less stable per O atom than the ideal $TiO_2(110)$ surface plus a free O_2 molecule. In other words, the adsorbed O atoms may recombine with each other on the $TiO_2(110)$ surface to form O_2 if the O atoms can diffuse quite fast with small barriers, given their relatively weaker bonding to the surface. It is thus important to elucidate the mobility of O atoms on the surface, to distinguish two possible O_2 evolution mechanisms: direct recombination of two adsorbed O atoms or further oxidation of the OOH intermediate.

C. Mobility of Adsorbed O Atoms on the $TiO_2(110)$ Surface. Eight transition structures, **a/a**, **a/b**, **a/c**, **b/e′**, **e/e**, **d/e′**, **e/e′**, and **c/e′**, are found in our calculations, each labeled by a slash between the two minima with which the transition structure is connected (Figure 3). These transition structures can be classified into two groups according to whether an O−O single bond is breaking. Let us look at the transition structures not involving O−O bond breaking first, which include **a/a**, **b/e′**, **d/e′**, and **e/e′**. The transition structure **a/a** is related to the diffusion of the O adatom along the surface Ti_{5c} trough, which has a potential barrier of 0.57 eV at $^1/_2$ ML coverage. The two equal Ti−O bonds (2.014 Å) are evidently longer than that found in **a**, and the energy of transition state **a/a** is even 0.11 eV higher than that of the free slab plus the O(^{3}P) atom. At $^1/_3$ ML coverage, transition structure **a/a** is still 0.10 eV higher in energy than the dissociation limit, leading to an even higher O-atom diffusion barrier of 0.83 eV. This means that the elimination of O adatom is easier than its direct diffusion along the surface Ti_{5c} trough, effectively ruling out this mechanism for O-atom surface diffusion. The transition structures of **c/e′**, **d/e′**, and **e/e′** are all related to flexible motions of the O adatom bound to a bridging oxygen O_b and associated with some low potential barriers (lower than 0.4 eV), with **e′** as the key intermediate. By use of the so-called nudged elastic band method, the direct transition barrier from **c** to **d** is estimated to be about 1.0 eV in other recent DFT calculations.[21−23] However, starting from the inferred[21] transition structure **c/d**, we always get **c/e′** with a lower barrier of 0.34 eV above **c** instead, suggesting that structure **c/d** is a second-order saddle point rather than a true transition state in nature. Moreover, transition structure **d/e′** represents a low **e′** → **d** transition barrier of only 0.16 eV (or 0.38 eV for the reverse **d** → **e′** transition); this means that **d** can be reached from **c** involving two transition states (**c/e′** and **d/e′**), of which the highest lies only 0.34 eV above **c**. Finally, the transition structure **e/e′** has essentially the same potential energy as configuration **e**, suggesting that the O adatom moves quite freely around the O_b site to which it binds.

When the breaking of a peroxide O−O bond is involved, as shown in the transition structures **a/b**, **a/c**, **b/e′**, and **e/e**, high potential barriers (higher than 0.9 eV) are generally observed from stable surface peroxide species such as **b**, **c**, **e**, and **e′**. On the other hand, transition structures **a/b** and **a/c** are related to the "capture" events of O_{ip} and O_b atoms, respectively, by the terminal O adatom on the Ti_{5c} trough site. The respective **a** → **b** and **a** → **c** transition barriers are 0.28 and 0.58 eV, suggesting that an in-plane O_{ip} is more easily "captured" by the terminal O adatom on the Ti_{5c} trough site than an O_b atom. Further motion of the O adatom from O_{ip} toward O_b via transition structure **b/e′** is associated with a high barrier of 1.23 eV. Finally, the transition structure **e/e** is related to the diffusion of the O adatom along the surface O_b ridge with a high barrier of 0.91 eV.

For clarity, the O-atom diffusion pathways on the $TiO_2(110)$ surface are shown schematically in Figure 4. Note that the relevant diffusion pathways along the [001] direction (Figure 4a) or the [−110] direction (Figure 4b) involve at least one of the transition states **a/a**, **a/b**, and **e/e** or **a/c** and **b/e′**, respectively. Since water molecules are most likely bound to surface Ti_{5c} via O → Ti_{5c} donative bonds, it is natural to assume configuration **a**, with a terminal Ti−O bond, as the initial adsorption state of the O atom after two protons are removed from water during photoelectrolysis. Starting from this configuration, direct O-atom diffusion along the Ti_{5c} trough through **a/a** and direct association with surface O_b through **a/c** are unlikely due to barriers higher than the dissociation limit, while the association with surface O_{ip} leading to stable configuration **b** through **a/b** is possible over a low barrier of about 0.3 eV. If there is no

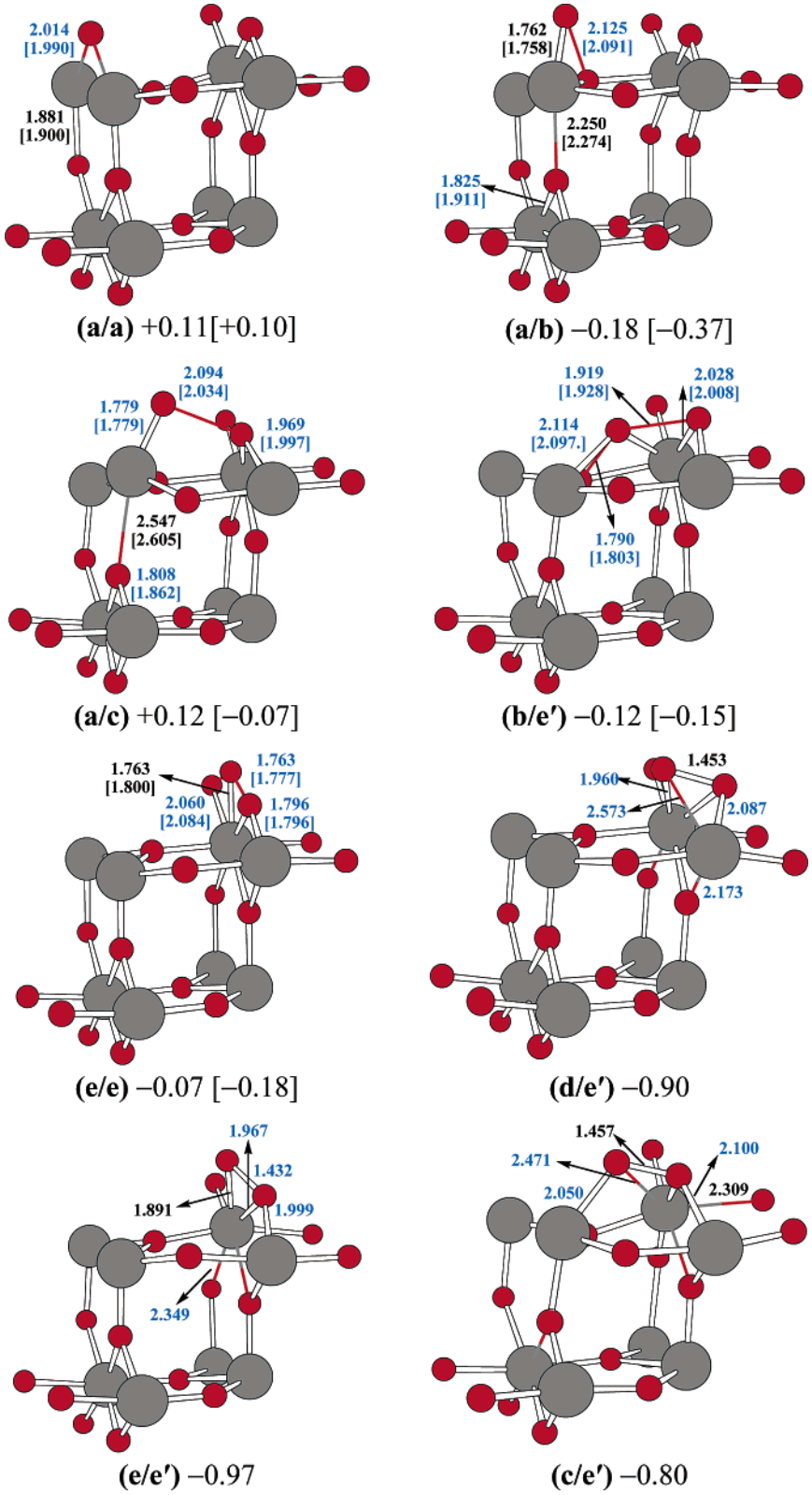

Figure 3. Optimized geometries (two top trilayers, in angstroms) and potential energies (in electronvolts) of the transition structures for a single O(^{3}P) adatom on the 2 × 1 and 3 × 1 (in brackets) rutile (110) surface unit cells. The structure between **a** and **c** is labeled as **a**/**c**, and so on.

energy dissipation to the TiO_2 bulk, further diffusion of O atom along both the [001] and the [−110] directions would in principle be possible via the sequences of **a** ↔ **b** ↔ **a** and **a** ↔ **b** ↔ **e**′ ↔ **e** ↔ **e**′ ↔ **b** ↔ **a**, respectively. However, the diffusion of O atoms with liquid water on the TiO_2 surface will presumably be hindered by the high **b** → **a** and **b** → **e**′ barriers of about 1 eV, and thus the O atom is most likely to end up in the stable peroxide configuration **b**. Furthermore, if the photoelectrolysis of water is initiated by a nucleophilic attack of H_2O molecules on surface-trapped holes on surface oxygen sites, as proposed recently,[13−15] the energetically very close peroxide configurations **c**, **d**, **e**, and **e**′ are also possible adsorption states

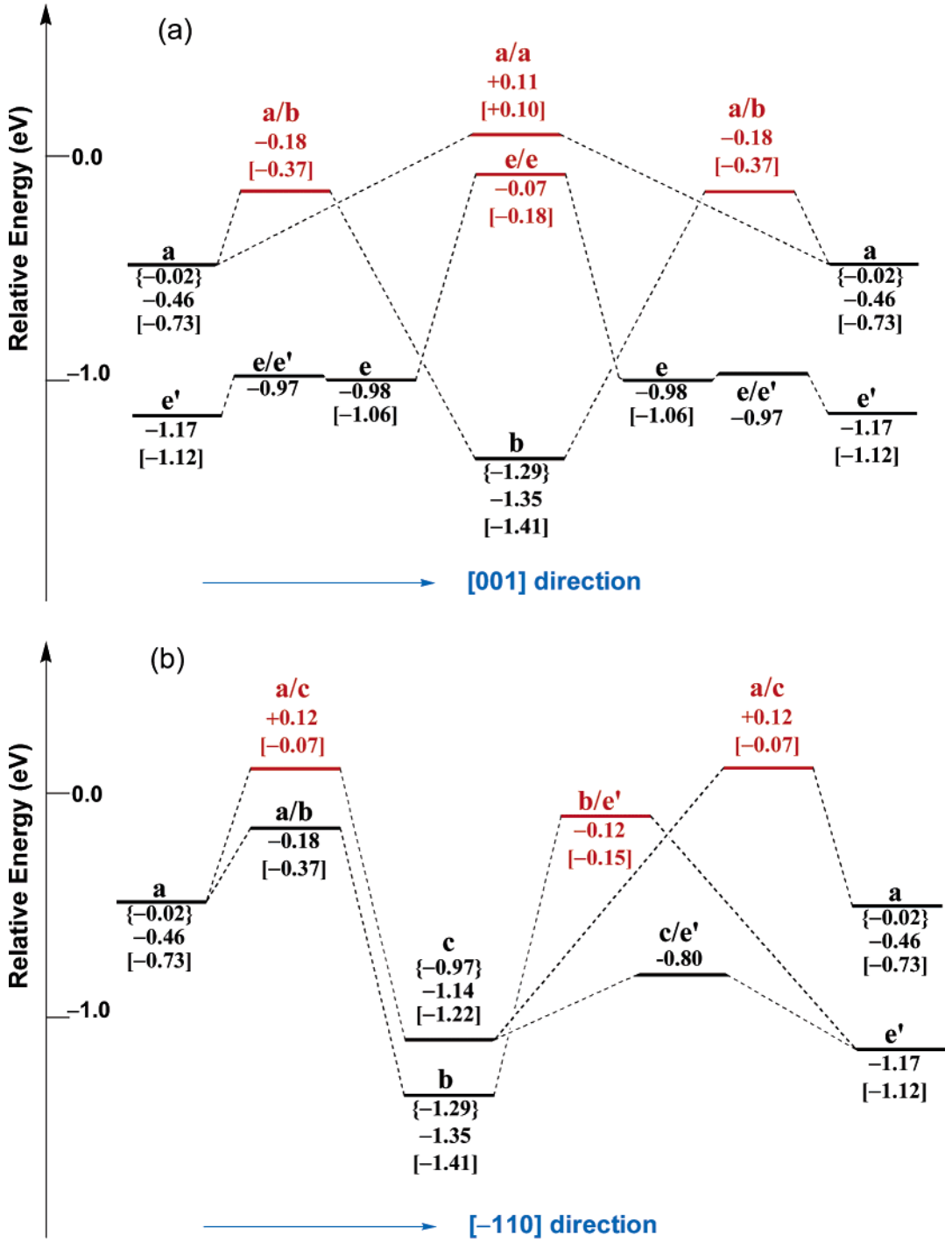

Figure 4. Schematic O-atom diffusion pathways on the rutile (110) surface along the (a) [001] and (b) [−110] directions. Relative energies (in electronvolts) are taken from Figures 2 and 3. The most relevant transition structures on the pathways are indicated in red.

of the O atom on the surface, but the further diffusion of O atom is again unlikely due to high **c** → **a** and **e** → **e** barriers involving O−O bond breaking.

D. Effects of Coadsorbed Water on Adsorption of O Atoms. Using the 2 × 1 surface unit cell, we have also examined the effects of one coadsorbed water (H_2O) molecule on the O-atom adsorption energies of configurations **a**−**e**. Such new configurations with coadsorbed water, as shown in Figure 5, are labeled by appending an additional letter **w** to the original configuration labels. At $^1/_2$ ML coverage of molecular H_2O on TiO_2(110) (see panel **w**), the water molecule binds on a Ti_{5c} site with a long O···Ti_{5c} bond (2.349 Å) and an additional H···O_b hydrogen bond (2.078 Å), and the calculated H_2O adsorption energy is 0.48 eV. At 1 and $^1/_3$ ML coverages the molecular H_2O adsorption energies are 0.54 and 0.52 eV, respectively. The molecular H_2O adsorption is found to be 0.08 eV less stable at $^1/_3$ ML coverage but 0.04 and 0.25 eV more stable at higher $^1/_2$ and 1 ML coverages, respectively, than its dissociative adsorption to form one terminal and one bridging OH group. This observation agrees very well with recent RPBE results[18] but differs from recent PW91 results,[16] which found preferred molecular H_2O adsorption for all coverages.

Here we consider only the coadsorption of O and molecular H_2O on TiO_2(110), both with $^1/_2$ ML coverage. In all cases the relaxed slab with water adsorbed on it plus the free O atom is taken as zero energy. In most cases, the bonding features of

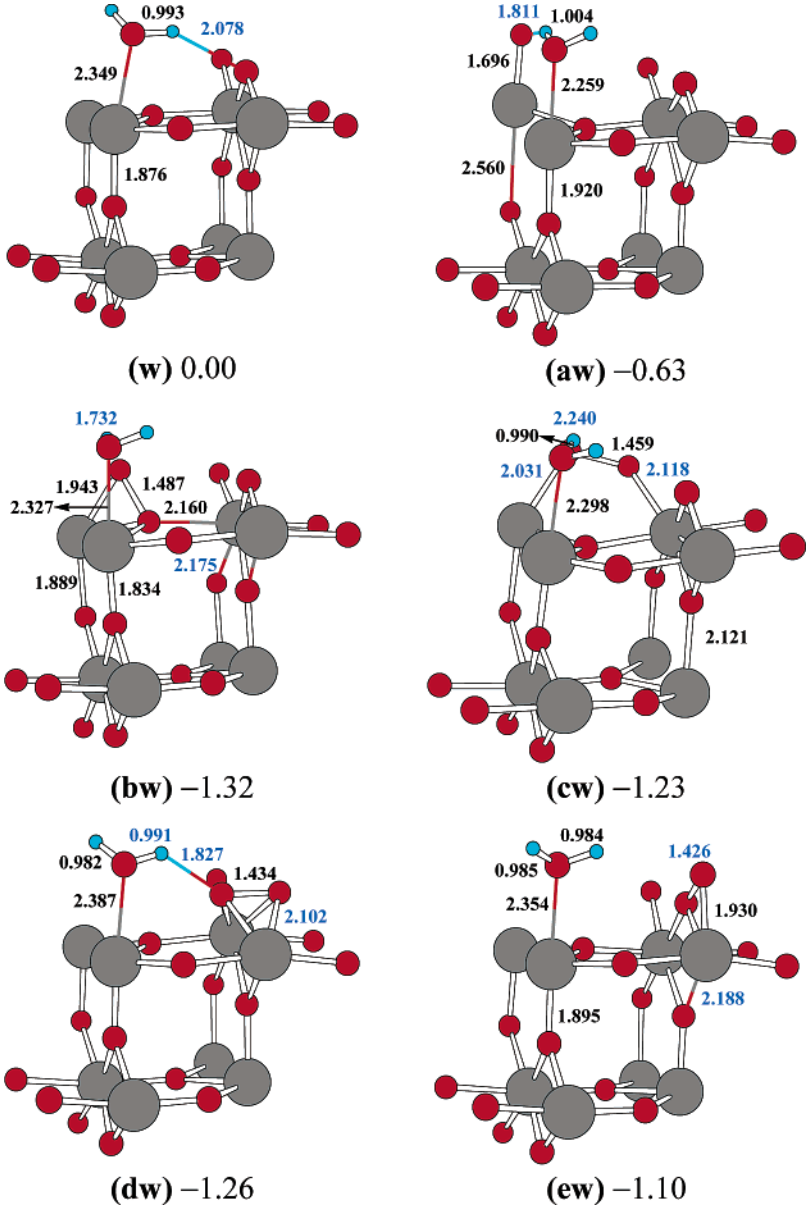

Figure 5. Optimized geometries (in angstroms) and relative energies (in electronvolts) on the rutile (110) surface with coadsorbed water and the 2×1 surface unit cell. The two fixed bottom trilayers of the four-layer model slab are omitted for simplicity. The relaxed slab with water adsorbed on it plus a free $O(^3P)$ atom is taken as zero energy.

H_2O and O are not changed much by coadsorption, except for possible new hydrogen bonds between them instead of the old hydrogen bond between H_2O and surface bridging O_b atoms. For example, there is a shorter and thus stronger hydrogen bond (H···O distance 1.811 Å) between H_2O and the O adatom than that observed in **w**, which stabilizes the terminal-O configuration **a** slightly (by 0.17 eV), with a higher O-binding energy of 0.63 eV. The largest structural changes are observed for the configuration **bw**, where one very short hydrogen bond (H···O distance 1.732 Å) between H_2O and the O adatom is formed at the price of breaking one old Ti−O bond between the O adatom and the Ti_{5c} atom, which has now become a H_2O binding site. As a result, the O-atom adsorption energy (1.32 eV) in configuration **bw** remains roughly the same as that in **b**. The calculated O-atom adsorption energies of 1.23, 1.26, and 1.10 eV in configurations **cw**, **dw**, and **ew** are also very close to the values of 1.14, 1.30, and 0.98 eV as found in the H_2O-free configurations **c**, **d**, and **e**, respectively. In short, water coadsorption has only minor effects on O-atom adsorption on TiO_2(110).

According to our calculations, the peroxide adsorption configurations of the O atom, **b**−**e**, are about 0.5−0.7 eV more stable than the terminal-O configuration **a**, regardless of whether a coadsorbed water molecule is present. However, only the less stable configuration **aw** is assumed for the coadsorption of molecular H_2O and O atoms in the only recent DFT study of this topic.[27] Even for this terminal-O configuration **(aw)**, we notice an important difference between our calculation and the recent DFT study[27] (with CASTEP package) concerning the nature of the O adatom. We find that spin-polarization has no effects on the O-atom adsorption energy in the terminal-O configuration regardless of whether a coadsorbed water molecule is present, while a spin density of 1.1e on the O adatom is found for the coadsorption configuration (**aw**) in the recent DFT study.[27] However, addressing the same issue, ref 21 noted some doubts about the quality of the pseudopotentials in the CASTEP package. Unfortunately, there are no experimental data on the structure **aw**, possibly due to the lower stability of such a terminal-O structure as compared with other surface peroxide

species. Noticing that spin-polarization was also found to be unimportant for the terminal-O configuration **a** in other recent DFT studies[21−24] and that the coadsorbed closed-shell H_2O molecule should have minor effects on the bonding features of O to the surface except for the possibility of forming a hydrogen bond between H_2O and the O adatom, we believe our results are reasonable. Furthermore, our calculated terminal bond length (1.696 Å) is also consistent with a Ti═O double bond rather than a Ti−O• single bond (∼1.9 Å).

Since the first 1 ML H_2O is the most tightly bound to the TiO_2 surface,[17,43] it should be the most relevant substrate for photolysis. As seen above, the interaction between a first-layer H_2O molecule and O does not change O-adsorption energies much (within 0.1 eV) as compared with the values calculated without water. We thus expect that additional water molecules or layers will also not change the calculated O-atom adsorption energies much. On the other hand, the steric hindering effects of additional water molecules could make the diffusion of O atoms on the TiO_2 surface more difficult. Diffusion of O atom on bare TiO_2 is already difficult, according to our calculations, and additional water molecules would further enhance this difficulty. Given the difficulty of O-atom diffusion on the TiO_2-(110) surface, our results suggest that the experimentally observed surface peroxide species Ti−O−O−Ti is due to *adsorbed O-atom* intermediates, rather than the proposed[13−15] coupling between two terminal Ti−O radicals. Further detailed study on the effects of multilayer water could yield additional insight but is not expected to alter our main conclusions.

IV. Conclusions

We have investigated the adsorption of oxygen atoms [O(^{3}P)] on both the ideal and the hydrated rutile TiO_2(110) surface using periodic DFT calculations within the RPBE generalized gradient approximation and four Ti-layer slabs, with (2 × 1) and (3 × 1) surface unit cells. Conclusions are as follows:

1. The ideal TiO_2(110) surface has alternately shortened and elongated Ti−O bonds in the [110] direction in the top layers as compared with TiO_2 bulk.

2. On both the ideal and hydrated TiO_2 surfaces, O atoms are adsorbed as stable peroxide TiOOTi species rather than as terminal Ti═O and O−O species.

3. Upon adsorption on TiO_2(110), the spin of O(^{3}P) atom is completely lost, opposing the concept of a surface Ti−O• radical intermediate.

4. Diffusion of O atoms on TiO_2(110) is hindered by a high barrier of about 1 eV due to the requirement of breaking a peroxide O−O bond, although the O adatom moves quite freely around the bridging-O site to which it binds.

5. On ideal TiO_2(110), H_2O may be adsorbed molecularly at high coverages but dissociatively at low coverages.

6. Changes in the O-atom coverage ratio and coadsorption with H_2O have only minor effects on the O-atom adsorption energies of stable peroxide configurations.

7. Our results rule out the O_2 evolution mechanism of direct recombination of O atoms on TiO_2(110), suggesting instead that an O atom adsorbed as a spinless peroxide species may be an important intermediate in photoelectrolysis of water.

Acknowledgment. This work was supported by the NWO/ACTS hydrogen program. Z.-w.Q. thanks Dr. J. Rossmeisl and Professor J. K. Nørskov for a fruitful work visit and help with the DACAPO program in the ASE package.

References and Notes

(1) Grätzel, M. *Nature (London)* **2001**, *414*, 338.
(2) Fujishima, A.; Honda, K. *Nature (London)* **1972**, *238*, 37.
(3) Volodin, A. M. *Catal. Today* **2000**, *58*, 103.
(4) Umebayashi, T.; Yamaki, T.; Itoh, H.; Asai, K. *Appl. Phys. Lett.* **2002**, *81*, 454.
(5) Ohno, T.; Mitsui, T.; Matsumura, M. *Chem. Lett.* **2003**, *32*, 364.
(6) Khan, S. U. M.; Al-Shahry, M.; Ingler, W. B., Jr. *Science* **2002**, *297*, 2243.
(7) Sakthivel, S.; Kisch, H. *Angew. Chem., Int. Ed.* **2003**, *42*, 4908.
(8) Paulose, M.; Mor, G. K.; Varghese, O. K.; Shankar, K.; Grimes, C. A. *J. Photochem. Photobiol. A: Chem.* **2006**, *178*, 8.
(9) Hoffmann, M. R.; Martin, S. T.; Choi, W.; Bahnemann, D. *Chem. Rev.* **1995**, *95*, 69.
(10) Muscat, J.; Swamy, V.; Harrison, N. M. *Phys. Rev. B* **2002**, *65*, 224112.
(11) Diebold, U. *Surf. Sci. Rep.* **2002**, *293*, 1.
(12) Thompson, T. L.; Yates, J. T., Jr. *Top. Catal.* **2005**, *35*, 197.
(13) Nakamura, R.; Nakato, Y. *J. Am. Chem. Soc.* **2004**, *126*, 1290.
(14) Nakamura, R.; Okamura, T.; Ohashi, N.; Imanish, A.; Nakato, Y. *J. Am. Chem. Soc.* **2005**, *127*, 12975.
(15) Nakamura, R.; Imanish, A.; Murakoshi, K.; Nakato, Y. *J. Am. Chem. Soc.* **2003**, *125*, 7443.
(16) Harris, L. A.; Quong, A. A. *Phys. Rev. Lett.* **2004**, *93*, 086105.
(17) Zhang, C.; Lindan, P. J. D. *J. Chem. Phys.* **2003**, *119*, 9183.
(18) Lindan, P. J. D.; Zhang, C. *Phys. Rev. B* **2005**, *72*, 075439.
(19) Schaub, R.; Wahlstrom, E.; Ronnau, A.; Lægsgaard, E.; Stensgaard, I.; Besenbacher, F. *Science* **2003**, *299*, 377.
(20) Henderson, M. A.; Epling, W. S.; Perkins, C. L.; Peden, C. H. F.; Diebold, U. *J. Phys. B* **1999**, *103*, 5328.
(21) Rasmussen, M. D.; Molina, L. M.; Hammer, B. *J. Chem. Phys.* **2004**, *120*, 988.
(22) Tilocca, A.; Selloni, A. *ChemPhysChem* **2005**, *6*, 1911.
(23) Wang, Y.; Pillay, D.; Hwang, G. S. *Phys. Rev. B* **2004**, *70*, 193410.
(24) Wu, X.; Selloni, A.; Lazzeri, M.; Nayak, S. K. *Phys. Rev. B* **2003**, *68*, 241402.
(25) Wendt, S.; Schaub, R.; Matthiesen, J.; Vestergaard, E. K.; Wahlström, E.; Rasmussen, M. D.; Thostrup, P.; Molina, L. M.; Lægsgaard, E.; Stensgaard, I.; Hammer, B.; Besenbacher, F. *Surf. Sci.* **2005**, *598*, 226.
(26) Perkins, C. L.; Henderson, M. *J. Phys. Chem. B* **2001**, *105*, 3856.
(27) Zhang, C.; Lindan, P. J. D. *J. Chem. Phys.* **2004**, *121*, 3811.
(28) Hammer, B.; Hansen, L. B.; Nørskov, J. K. *Phys. Rev. B* **1999**, *59*, 741.
(29) Vanderbilt, D. *Phys. Rev. B* **1990**, *41*, 7892.
(30) Payne, M. C.; Teter, M. P.; Allan, D. C.; Arias, T. A.; Joannopoulos, J. D. *Rev. Mod. Phys.* **1992**, *64*, 1045.
(31) Kresse, G.; Furtmüller, J. *Comput. Mater. Sci.* **1996**, *6*, 15.
(32) An open source code of the DACAPO program and the ASE package is available at the web page https://wiki.fysik.dtu.dk/ase.
(33) Vinet, P.; Ferrante, J.; Smith, J. R.; Rose, J. H. *J. Phys. C* **1986**, *19*, L467.
(34) Hameeuw, K. J.; Cantele, G.; Ninno, D.; Trani, F.; Iadonisi, G. *J. Chem. Phys.* **2006**, *124*, 024708.
(35) Culot, P.; Dive, G.; Nguyen, V. H.; Ghuysen, J. M. *Theor. Chim. Acta* **1992**, *82*, 89.
(36) *CRC Handbook of Chemistry and Physics*, 82nd ed.; Lide, D. R., Ed.; CRC Press: Boca Raton, FL, 2002.
(37) Kurth, S.; Perdew, J. P.; Blaha, P. *Int. J. Quantum Chem.* **1999**, *75*, 889.
(38) Lindsay, R.; Wander, A.; Ernst, A.; Montanari, B.; Thornton, G.; Harrison, N. M. *Phys. Rev. Lett.* **2005**, *94*, 246102.
(39) Qu, Z.-W.; Kroes, G.-J. *J. Phys. Chem. B* **2006**, *110*, 8998.
(40) Schaub, R.; Thostrup, P.; Lopez, N.; Lægsgaard, E.; Stensgaard, I.; Nørskov, J. K.; Besenbacher, F. *Phys. Rev. Lett.* **2001**, *87*, 266104.
(41) Rossmeisl, J.; Logadottir, A.; Nørskov, J. K. *Chem. Phys.* **2005**, *319*, 178.
(42) Reuter, K.; Scheffler, M. *Phys. Rev. B* **2001**, *65*, 035406.
(43) Kornherr, A.; Vogtenhuber, D.; Ruckenbauer, M.; Podloucky, R.; Zifferer, G. *J. Chem. Phys.* **2004**, *121*, 3722.